


 Cite this: *RSC Adv.*, 2021, 11, 17377

Metal oxide adsorption on fullerene C₆₀ and its potential for adsorption of pollutant gases; density functional theory studies†

 Sanaz Haghgoo  and A.-Reza Nekoei*

Combinations of fullerene and metal oxides (MOx) are interesting, not only because they display the individual properties of fullerene and of MOx nanoparticles, but they may also exhibit synergetic properties that are advantageous for gas sensing applications. In the present work, the adsorption of some different MOx on fullerene C₆₀, and also the NO₂ and CO sensing properties of these complexes, have been theoretically studied. All quantum mechanical computations have been carried out using Gaussian G09, employing the DFT method at the B97D/6-311G(d,p) level. NBO theory has been used for analysis of the charge transfers during gas adsorption. The chemical nature of the newly formed bonds in the studied complexes and their relative strength have been analysed using AIM2000 software. The results show that MOx/C₆₀ complexes are much stronger adsorbents for NO₂ and CO than C₆₀ is. It is also expected that these complexes have more optical and electrical sensitivity in the selectivity towards gases, including NO₂ and CO.

Received 21st March 2021

Accepted 5th May 2021

DOI: 10.1039/d1ra02251b

rsc.li/rsc-advances

1 Introduction

Metal oxides (MOx) are widely used in environmental reconstruction and destruction of organic pollutants due to their easy accessibility, low cost and non-toxicity and excellent photocatalytic properties.^{1–4} In the photocatalytic processes, the absorbed photons in MOx form electron–hole pairs, which can react with molecules on the surface of particles and cause their destruction or degradation. Despite the high ability of MOx to perform photocatalytic processes, some limitations prevent their widespread use in these processes. Their relatively low quantum efficiency due to the quick recombination of electron–hole pairs is among the limitations of most MOx, especially titanium dioxide (TiO₂) and is a limiting factor in photocatalytic processes.⁵ The photocatalytic activity of MOx is improved by some modifications such as coupling with other elements, and surface coating with noble metals and other semiconductors.^{6,7}

Conjugation of the MOx with three-dimensional π systems effectively enhances the electron transfer process between them.⁸ Fullerenes C₆₀, with spherical closed-shell configuration consisting of 30 bonding molecular orbitals with 60 π -electrons,⁹ is suitable for conjugation with the MOx that improves the electron transfer process and leads to the reduction of C₆₀ and minimization of the structural changes.^{10,11} One of the remarkable properties of the fullerenes (with a high electron-

acceptor capacity) in the electron transfer processes is their ability to the quick separation of photoinduced charges, and consequently slows down the electron–hole pair recombination.¹² Therefore, conjugation of the MOx and fullerene C₆₀ provides an ideal system for more efficient electron transfer and charge separation.

MOx, especially ZnO, have been highly regarded in the field of gas monitoring due to the high mobility of conduction electrons and their chemical and thermal stability. Detecting properties for various gases including toxic and pollutant gases (such as CO, NO_x, H₂S and SO₂) by MOx nanoparticles have been reported in many studies.^{13–15} However, some factors like photo corrosion processes^{16,17} and the high HOMO–LUMO energy gap^{18,19} for the MOx decrease their activity and stability, and limit their application in the gas monitoring. In addition, the operating temperature of these detectors is high, that leads to the high energy consumption and security problems related to the presence of explosive gases in the environment.²⁰

Interactions between the MOx and fullerenes can change the bond gaps of the reactants, and thereby change conductivity of the total system. The study on optical conductivity of the complex of fullerene C₆₀ and TiO₂ shows that its conductivity has been significantly increased in presence of radiation.²¹ Interaction between the zinc oxide particles and fullerene C₆₀ enhances stability of the ZnO nanostructure in addition to increase efficient photocatalytic activities.²² Moreover, fullerene has a high surface area that can provide more situations for more effective processes. It has been also shown that interaction between the TiO₂ nanoparticles and fullerene C₆₀ reduces toxicity of the C₆₀ in aquatic environments.²³

Department of Chemistry, Shiraz University of Technology, Shiraz, 71555-313, Iran.
E-mail: nekoei@sutech.ac.ir; Tel: +98-07137354501-7

† Electronic supplementary information (ESI) available. See DOI:10.1039/d1ra02251b



Therefore, studying and understanding the interactions between the MOx and fullerenes is particularly important. The researches in scientific sources express that such interactions have been only investigated for the TiO₂ and ZnO crystalline nanoparticles.^{21–23} Nonetheless, investigating of the interactions between the MOx and fullerenes at the molecular levels, understanding behaviour of the orbitals, gaining the energies and other adsorption parameters are only possible through the theoretical calculations and molecular quantum studies, which, based on our literature survey, has not been performed, yet.

In this study, molecular interactions between the ZnO (n-type semiconductor), NiO and Cu₂O (p-type semiconductors) MOx with the fullerene C₆₀ (n-type) have been theoretically studied. Adsorption energies, intermolecular distances in complex structures of the fullerene-MOx (MOx/C₆₀), energy of HOMO–LUMO surfaces and their gap, NBO charges analyses, enthalpy changes, polarizabilities and some reactivity indices in these interactions have been analysed and compared with each other.

Since the adsorbed MOx on the fullerene C₆₀ almost change the conductivity, dipole moment and the other electronic properties of the C₆₀, it is expected that the MOx/C₆₀ complexes will behave different from the involved molecules (C₆₀ and MOx) in variety of the reactions including interactions with the gases.

On the other hand, the studies on adsorption and storage of the gas molecules by the fullerene C₆₀ show that the gases such as N₂, Ar and CO₂ locate in the inter-cavity spaces of this spherical structure. Nevertheless, they are weakly adsorbed on the surface of C₆₀.²⁴ This, besides the weak adsorption of gases like CO, NO, CO₂ and N₂O on the fullerene surface, indicates that the unmodified surface of the C₆₀ is not suitable for adsorption or storage of these gases.^{25,26}

One of the modifications that improves the gas detection ability of the carbon structure substrates is their combination with single metal atom catalysts.²⁷ The carbon substrates doped with the single atom catalysts based on transition metal atoms can effectively alter the surface's local electrical neutrality and increase effective reaction sites.^{27–32} For example, Luo *et al.* showed that fullerenes doped with MnN₄ catalyst efficiently adsorb toxic gases. Nevertheless, this substrate (MnN₄-C₆₀) is incapable in oxidizing gases.²⁷ Oxidation of a toxic gas is a significant advantage for its sensing. MOx/C₆₀ adsorbents are predicted to provide oxidation potential of toxic gases due to the presence of oxygen in their structure, in addition to their more efficient gas adsorption. Another advantage is more availability of the substrates and less difficulty of the synthesis. MnN₄-C₆₀ substrates (MnN₄ doping for C atoms of C₆₀) require more time and knowledge for its synthesis, compared to that of the MOx/C₆₀ exohedral fullerene adsorbents.

Based on our literature survey, there is no experimental or theoretical investigation on gas adsorption on MOx/C₆₀ complexes. Studying adsorption of the NO₂ (electrophile) and CO (nucleophile) gases on the MOx/C₆₀, is another purpose of this research and could be useful in gaining the detectors with higher sensitivity and capability. NO₂ is one of the pollutants of which million tons is produced every year, and its most

important sources are internal combustion engines, thermal power plants and to some extent pulp factories. Inhalation of the NO₂ gas is toxic, and long-term exposure to that has adverse effects on health.^{33,34} CO is another common gas pollutant, which is produced during the combustion processes, and has adverse effects on human health and environment. Although many efforts have been made to reduce these gas pollutants,^{35,36} more effective methods are still needed to eliminate them.

2 Computational methods

In the weaker interactions, such as interaction of the gases on the fullerene surfaces, dispersion forces or van der Waals forces play a major role.³⁷ One of the DFT based methods that includes dispersion forces in computations is B97D (or Grimm method involving dispersion).³⁸ In this method, the generalized gradient approximation (GGA) is used to calculate the exchange-correlation energy and can comprise electronic long-range correlations (which are responsible for the van der Waals forces) in the calculations.³⁸

The geometries of all free structures, including the fullerene C₆₀, MOx, and NO₂ and CO gases, in addition to the complexes of their interactions have been fully optimized at the B97D/6-311G(d,p) theoretical level. Harmonic vibration frequency calculations have been also performed following the geometrical optimizations to confirm the global minimums, at the same method and basis set. Interaction energies have been calculated for all complex systems and these energies have been corrected for the basis set superposition error (BSSE).^{39,40} All optimizations and energy calculations in this study have been carried out using Gaussian W09 package.⁴¹

Analyses of natural bond orbitals (NBOs) have been done using GENNBO 5.0 software⁴² to investigate the natural atomic charges, charge transfers between donor–acceptor bond orbitals, and the interaction energies between them. Gauss View 5.0 software⁴³ has been also used to visualize and investigate geometries and structural properties.

Chemical nature of new formed bonds in the studied complexes and their relative strength have been analysed using Atoms in Molecules (AIM) theory of Bader.^{44,45} Electron density ($\rho(r_c)$) at the critical points of the bonds and its Laplacian ($\nabla^2\rho(r_c)$) for the global minimum structures have been estimated using AIM2000 software.⁴⁴ The magnitude and sign of

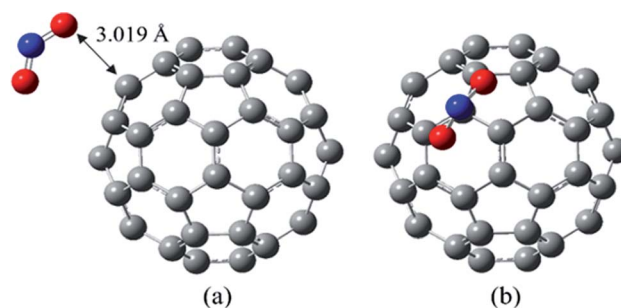


Fig. 1 The most stable complex of NO₂/C₆₀ in two different views, at B97D/6-311G(d,p).

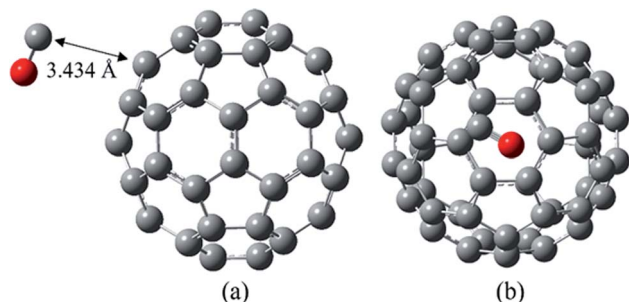


Fig. 2 The most stable complex of CO/C₆₀ in two different views, at B97D/6-311G(d,p).

Table 1 N–O/C–O bond lengths (in Å) and Wiberg bond orders of NO₂, CO and the most stable complexes of NO₂/C₆₀ and CO/C₆₀, calculated at B97D/6-311G(d,p) level

Structure	Bond	Bond length	Bond order
NO ₂ /C ₆₀	N–O	1.205	1.642
CO/C ₆₀	C–O	1.137	2.293
NO ₂	N–O	1.203	1.650
CO	C–O	1.136	2.298

the electron density's Laplacian by specifying condensation or expulsion zones of charges is the basis for categorizing the nature of interactions.⁴⁵ Laplacian values of ρ at the r_c for atomic interactions in molecules at the equilibrium geometries have a negative sign for the systems with covalent interactions; and have relatively small values with a positive sign for weak closed-shell interactions such as van der Waals interactions.⁴⁵

3 Results and discussion

3.1 Gases adsorption on fullerene C₆₀

Structural study. The NO₂ and CO gas molecules have been placed in different sites of the fullerene C₆₀, and the calculated structures of the most stable complexes have been shown in Fig. 1 and 2, respectively.

Calculated values of bond lengths and Wiberg bond orders for N–O and C–O bonds of the most stable complexes of NO₂/C₆₀ and CO/C₆₀, together with their corresponding values for the NO₂ and CO gas molecules have been listed in Table 1. Absolute

energies ($E_{\text{abs.}}$), also their corrected values for zero point energy (ZPE), of NO₂, CO and their most stable complexes with C₆₀ have been given in ESI as Table S1.†

According to the optimization calculations, those NO₂/C₆₀ complexes are the most unstable in which the NO₂ group has interacted with the C₆₀ from the nitrogen atom side. In the most stable complex of NO₂/C₆₀, the NO₂ molecule has interacted with the C₆₀ by its oxygen atoms. As shown in Fig. 1, in this structure, one of the oxygens has placed on a pentagonal ring and the other has located on a hexagonal ring of the C₆₀.

The value of 3.019 Å has been obtained for the shortest distance between the oxygen of the NO₂ and carbon atom of the C₆₀, with the Wiberg bond order of 0.010.

In the optimized NO₂ molecule, the N–O bond length and the ONO bond angle are 1.203 Å and 133.9°, respectively, which are very close to the experimental values (N–O bond length in the NO₂ molecule is 1.188 ± 0.004 Å, and the bond angle is $134.100 \pm 0.250^\circ$).⁴⁶ The obtained N–O bond length of NO₂ segment in the most stable complex of NO₂/C₆₀ is 1.205 Å, and its bond angle is 133.8°. In general, during the NO₂ adsorption on the C₆₀, the structural parameters of both molecules have not been significantly changed.

As shown in Fig. 2, in the most stable complex of CO/C₆₀ the CO molecule has almost located on a hexagonal ring of the C₆₀. The calculated distance of the carbon atom of the CO to the nearest carbon atom of the C₆₀ is 3.434 Å, with the Wiberg bond order of 0.010. According to the data of Table 1, the C–O bond length in the optimized CO molecule and also in the most stable complex of CO/C₆₀ is approximately 1.136 Å, at the B97D/6-311G(d,p) computational level. In general, it could be said that during the CO adsorption on the C₆₀, the structural parameters of both molecules have been unchanged.

AIM study. For the shortest distance between the oxygen of the NO₂ and carbon atom of the C₆₀ (Fig. 1), according to the AIM results, the small and positive value of the electron density's Laplacian $\nabla^2\rho$ (0.0285 a.u.) with the small value of electron density ρ (0.0089 a.u.) at the bond critical point between the two mentioned atoms indicates that their interaction is a very weak closed-shell of van der Waals type. At the critical point between the carbon atom of the CO to the nearest carbon atom of the C₆₀ (Fig. 2), the calculated value of 0.0080 and 0.0028 a.u. for the $\nabla^2\rho$ and ρ , respectively, indicates a van der Waals nature of this weak interaction.

Table 2 Adsorption energies and their values with the BSSE corrections, enthalpy changes of complexation, changes of NBO charges (Δq) in NO₂ and CO after complexation, energies of HOMO and LUMO levels and their gaps for C₆₀, NO₂, CO and the most stable complexes of NO₂/C₆₀ and CO/C₆₀, calculated at B97D/6-311G(d,p) level

Structure	$E_{\text{ads.}}$ (kcal mol ⁻¹)	$E_{\text{ads.}} + \text{BSSE}$ (kcal mol ⁻¹)	ΔH (kcal mol ⁻¹)	Δq (a.u.)	E_{HOMO} (eV)	E_{LUMO} (eV)	Gap (eV)
NO ₂ /C ₆₀	-3.93	-2.03	-2.78	-0.011	-5.72	-4.08	1.64
CO/C ₆₀	-2.15	-1.54	-4.73	0.000	-5.75	-4.09	1.66
NO ₂	—	—	—	—	-6.37	-3.45	2.91
CO	—	—	—	—	-8.96	-1.76	7.20
C ₆₀	—	—	—	—	-5.74	-4.08	1.66

Energy study. Values of the adsorption energies ($E_{\text{ads.}}$) with the BSSE corrections, enthalpy changes of the interactions, energies of the HOMO–LUMO levels and their gaps for the C_{60} , NO_2 and CO gases, and the most stable complex of NO_2/C_{60} and CO/C_{60} have been calculated and the results have been presented in Table 2.

The calculated $E_{\text{ads.}}$ values for adsorption of the NO_2 and CO molecules on the C_{60} are small, and even smaller with the BSSE corrections. These, beside the small values of the enthalpy changes, confirm the weakness of these interactions, in agreement with the previously discussed results of structural and AIM studies.

According to the data in Table 2, the HOMO–LUMO levels and their gap in the fullerene C_{60} have been not or negligibly changed after adsorption of the studied gas molecules.

NBO study. According to the NBO charge calculations, the total changes in charge of the NO_2 and CO molecules after their adsorption on the C_{60} (given in Table 2, as Δq) are negligible, which again indicate that these interactions are very weak. In the case of NO_2 adsorption, the small negative value of charge transfer to NO_2 is due to its high electron acceptor property.⁴⁷

All structural, AIM, energy and NBO studies indicate that the adsorptions of the NO_2 and CO gas molecules on the C_{60} are very weak. Therefore, it is confirmed that fullerene alone cannot be a suitable adsorber or detector for the target gases.

3.2 Gases adsorption on the MOx

Structural study. In order to obtain the most stable complex structures of the NO_2/MOx and CO/MOx , all possible structures for placing of the NO_2 and CO molecules on the studied MOx have been considered, and the most stable structures have been

identified. These structures for the NO_2/MOx and CO/MOx have been shown in Fig. 3 and 4, respectively.

Also, the calculated values of the selected bond lengths and their Wiberg bond orders for the mentioned most stable complexes, together with those corresponding values of the MOx have been given in Table 3. The obtained $E_{\text{abs.}}$ values with the ZPE corrections for these complexes have been given in Table S1.†

According to Fig. 3(a), for the most stable structure of $\text{NO}_2/\text{Cu}_2\text{O}$ complex, each of the copper atoms has located in adjacent to one of the oxygen atoms of the NO_2 gas, with a distance of 1.907 Å and a bond order of 0.223. In the most stable structure of NO_2/ZnO complex, Fig. 3(b), ZnO has been approached to the oxygen atoms of NO_2 from the Zn side. This is in agreement with the findings of Spencer *et al.* in their theoretical study on adsorption of the NO_2 on the ZnO nanowires.⁴⁸ As shown in the Fig. 3 and Table 3, the distances of the Zn atom to the oxygen atoms are 1.960 and 2.290 Å. In the case of the most stable structure of NO_2/NiO complex, as shown in Fig. 3(c), NO_2 has interacted with the Ni atom more closely from its nitrogen side. Previously, Wang *et al.* studied adsorption of the NO_2 molecule on a surface of NiO using molecular simulation and DFT methods, and understood that the strongest interaction occurs when NO_2 approaches to the NiO surface from its N atom side.⁴⁹

According to the data in Table 3, the bond lengths of N–O in the structure of all NO_2/MOx complexes have been slightly increased in comparison to that in the NO_2 free molecule. The lengths of metal–oxygen bond of MOx in both complexes of $\text{NO}_2/\text{Cu}_2\text{O}$ and NO_2/ZnO are slightly higher than their corresponding values in the Cu_2O and ZnO molecules. These could be due to weak donor–acceptor interactions in the $\text{NO}_2/\text{Cu}_2\text{O}$

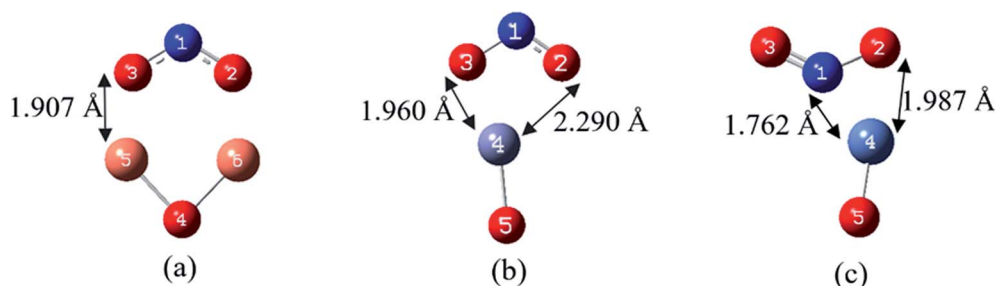


Fig. 3 The most stable complexes and the atom numbering of (a) $\text{NO}_2/\text{Cu}_2\text{O}$, (b) NO_2/ZnO and (c) NO_2/NiO , at B97D/6-311G(d,p).

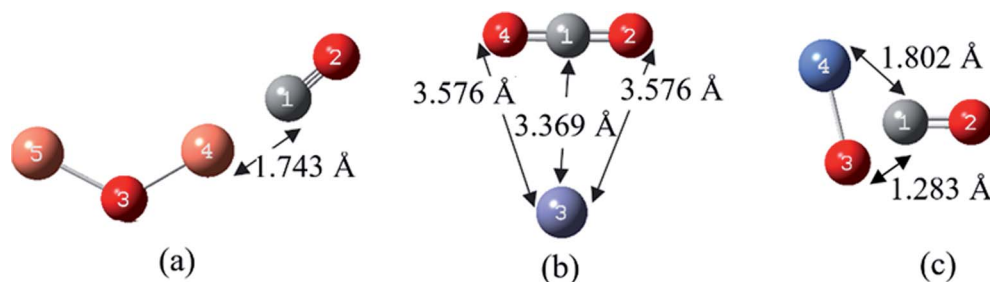


Fig. 4 The most stable complexes and the atom numbering of (a) $\text{CO}/\text{Cu}_2\text{O}$, (b) CO/ZnO and (c) CO/NiO , at B97D/6-311G(d,p).

Table 3 Bond lengths (in Å), Wiberg bond orders, in the most stable complexes of NO₂/MO_x and CO/MO_x and also MO_xs, calculated at B97D/6-311G(d,p) level

Structure	Bond	Bond length	Bond order
NO ₂ /Cu ₂ O	Cu5–O4, Cu6–O4	1.792	0.515
	Cu5–O3	1.907	0.234
	N1–O2, N1–O3	1.276	1.436
NO ₂ /ZnO	Zn4–O5	1.814	0.485
	Zn4–O2	2.290	0.133
	Zn4–O3	1.960	0.257
	N1–O2	1.238	1.630
	N1–O3	1.294	1.387
NO ₂ /NiO	Ni4–O5	1.629	1.094
	Ni4–O2	1.987	0.297
	Ni4–N1	1.762	0.503
	N1–O2	1.284	1.479
	N1–O3	1.193	1.471
CO/Cu ₂ O	Cu4–O3	1.751	0.434
	Cu5–O3	1.758	0.745
	Cu4–C1	1.743	0.834
	C1–O2	1.154	2.118
CO/ZnO	Zn3–O2, Zn3–O4	3.576	0.002
	Zn3–C1	3.369	0.015
	C1–O2, C1–O4	1.169	1.909
CO/NiO	Ni4–O3	1.820	0.527
	Ni4–C1	1.802	0.707
	C1–O3	1.283	1.384
	C1–O2	1.197	1.786
Cu ₂ O	Cu–O	1.766	0.795
	Cu–Cu	2.957	0.158
ZnO	Zn–O	1.776	0.992
NiO	Ni–O	1.673	1.030

and NO₂/ZnO complexes. Whereas for the most stable complex of NO₂/NiO, with the relatively good donor–acceptor interactions, the Ni–O bond length is shorter than that in the NiO molecule.

According to Fig. 4(a) at the most stable structure of CO/Cu₂O complex, the CO has been approached to the Cu atom from its carbon atom side, with a distance of 1.743 Å and a bond order of 0.834.

In the most stable form of CO/ZnO complex (Fig. 4(b)), interestingly, the adsorption is more a chemical interaction, which the CO molecule has adsorbed the oxygen atom of the ZnO, and thereby, a CO₂ molecule has been produced and Zn (with a partial charge of 0.009) released. The ZnO nanoparticles oxidize their adjacent species by creation of oxygen active species and have been always studied as a toxic MO_x in biological and health issues.^{50,51} The rapid and strong interaction of carbon monoxide gas on the MO_x substrate of ZnO and the releasing of CO₂ gas has been demonstrated in various experiments.⁵²

In the case of CO/NiO complex, the CO molecule has been approached to the NiO from its carbon side. The values of bond lengths and bond orders in this complex have been given in the Fig. 4(c) and Table 3. In this structure, the O3 of NiO is very close to the CO molecule and bonds with it (with a bond length of 1.283 Å and bond order of 1.384), but (unlike to the CO complex

with ZnO) its affinity for bonding with the Ni prevents releasing of CO₂.

According to the data in Table 3, the length of the CO bond in complex with the target MO_xs has become slightly longer than that in the free CO molecule (which is 1.136 Å). The metal and oxygen atoms distances of MO_xs in both complexes of CO/ZnO and CO/NiO are higher than their corresponding values in the ZnO and NiO molecules. However, for the complex of CO/Cu₂O, the Cu–O bond length is shorter than that in the Cu₂O molecule, which may be due to the notable donor–acceptor interaction from lone pair (LP) of O3 to σ* of C1–Cu4 bond (78.98 kcal mol^{−1}).

AIM study. The values of ∇²ρ for all bond critical points between the atoms involved in the interactions of gas molecules with metal oxides have been calculated. In the case of the NO₂/Cu₂O complex, no critical point has been detected by the AIM software at the distance between the NO₂ oxygen atoms and the Cu atoms (the involved atoms in the interaction in Fig. 3(a)). In the most stable complex of NO₂/ZnO, the calculated values of ∇²ρ at the critical points between the Zn atom to the O2 and O3 atoms (Fig. 3(b)) are 0.1433 (ρ = 0.0408 a.u.) and 0.4002 (ρ = 0.0876 a.u.), respectively. These values, together with the values of ∇²ρ and ρ at the critical point between Ni and nitrogen atoms in NiO/NO₂ (0.6491 and 0.1548 a.u., respectively), show significant van der Waals type interactions between the NO₂ gas molecule and the studied metal oxides.

According to the AIM calculations, in the most stable structure of CO/Cu₂O complex, the value of ∇²ρ at the critical point between Cu4 and carbon atom is 0.6340 (ρ = 0.1583 a.u.), which indicates a significant van der Waals type interaction between the two molecules. In the case of CO/ZnO, the ∇²ρ value at the critical point of the C1=O4 bonds (about −0.0174 with ρ = 0.4461 a.u.) can be considered as a confirmation of the covalent type interaction here. For the CO/NiO complex, the calculated ∇²ρ values at the critical points between the Ni–C and O3–C bonds are respectively 0.2945 (ρ = 0.1560 a.u.) and −0.3894 (ρ = 0.3466 a.u.). The negative value of ∇²ρ (with the acceptable value of ρ) indicates a covalent interaction between the CO molecule and the oxygen of NiO.

Energy study. The calculated adsorption energies, the enthalpy changes of complexation, energies of the HOMO–LUMO levels and their gaps for the MO_xs, and the most stable NO₂/MO_x and CO/MO_x complexes have been listed in Table 4.

In general, the calculated energies for adsorption of the NO₂ and CO on the studied MO_xs, in comparison with their adsorption on the C₆₀ (Table 2), show much larger values. In addition, the high values of enthalpy changes for adsorption of these gas molecules on the MO_xs, compared to those values in the C₆₀, are another confirmation of strength of these interactions. Enthalpy changes with a negative sign also indicate that these adsorption processes are exothermic. *E*_{ads} data in the Table 4 show that NiO is a much stronger adsorbent for the NO₂ and CO than the two other MO_xs.

According to the data in Table 4, the energy values of HOMO and LUMO levels and the gaps between them in the complexes of NO₂/MO_x and CO/MO_x have been significantly changed in comparison with those in the corresponding MO_xs.

Table 4 Adsorption energies and their values with the BSSE corrections, enthalpy changes of complexation, changes of NBO charges (Δq) in NO_2 and CO after complexation, energies of HOMO and LUMO levels and their gaps for the MOx, and the most stable complexes of NO_2/MOx and CO/MOx , calculated at B97D/6-311G(d,p) level

Structure	$E_{\text{ads.}}$ (kcal mol ⁻¹)	$E_{\text{ads.}} + \text{BSSE}$ (kcal mol ⁻¹)	ΔH (kcal mol ⁻¹)	Δq (a.u.)	E_{HOMO} (eV)	E_{LUMO} (eV)	Gap (eV)
$\text{NO}_2/\text{Cu}_2\text{O}$	-67.14	-41.50	-66.39	-0.717	-4.72	-3.07	1.64
NO_2/ZnO	-69.13	-59.37	-68.37	-0.655	-6.71	-3.43	3.28
NO_2/NiO	-134.70	-69.98	-133.42	-0.354	-6.25	-4.83	1.42
$\text{CO}/\text{Cu}_2\text{O}$	-55.60	-39.02	-54.10	-0.256	-3.64	-2.20	1.43
CO/ZnO	-130.43	-125.03	-127.73	0.468	-5.59	-0.21	5.39
CO/NiO	-134.44	-128.03	-132.60	0.089	-4.19	-3.00	1.20
Cu_2O	—	—	—	—	-3.23	-2.28	0.95
ZnO	—	—	—	—	-3.69	-3.60	0.09
NiO	—	—	—	—	-1.25	-0.59	0.66

NBO study. The NBO charge calculations on the complexes of NO_2/MOx have indicated that the total charge of NO_2 molecule has become negative after adsorption on the MOx, indicating the electron transfer from the MOx to the NO_2 . Amount of this charge transfer (Δq in Table 4) is very significant, compared to the amount of electrons that C_{60} transfers to NO_2 gas molecule during their interaction (-0.011 a.u.). According to the results of the previous section, the NiO interacts more strongly with the NO_2 compared to the other two MOx. Therefore, more charge transfer is expected during this adsorption process. However, according to the data in Table 4, the amount of charge that NO_2 receives from the NiO surface during their interaction is less than that of the other two MOx. This could be explained by considering the involved atoms in these interactions. As mentioned, NO_2 interacts with the NiO from its nitrogen side, and with the ZnO and Cu_2O from its oxygen atoms. Since nitrogen has less electronegativity than oxygen, NO_2 receives less electron from the NiO surface, compared to the ZnO and Cu_2O surfaces during adsorption on them.

According to the NBO calculation, the most notable donor-acceptor interactions in the complex of NO_2/NiO are from LP of

Ni4 to σ^* of N1-O3 (7.17 kcal mol⁻¹), and from LP of O5 to σ^* of N1-Ni4 (12.22 kcal mol⁻¹). In the case of the other two complexes ($\text{NO}_2/\text{Cu}_2\text{O}$ and NO_2/ZnO) no significant interaction is observed in the NBO calculations.

In the complex of $\text{CO}/\text{Cu}_2\text{O}$, 0.256 a.u. of charge has been transferred from Cu_2O to the CO unit (according to the NBO charges calculations), and the total charge of CO molecule has become negative after adsorption on the Cu_2O . The ZnO molecule has donated its oxygen atom to the CO during the interaction with it, and a neutral CO_2 molecule has been produced. The calculated initial charge of CO unit in the produced CO_2 molecule is 0.468 a.u., which indicates oxidation of CO against ZnO. In the complex of CO/NiO , the CO molecule has become similar to a CO_2 molecule by forming a new bond with the oxygen of NiO, but the tendency of this oxygen to keep a bond with the Ni has prevented releasing of CO_2 . Therefore, the oxidation process here is weaker than that in the CO/ZnO and is associated with lower charge transfer. In general, the charge transfer between the MOx and CO is much more significant compared to the amount of charge (near to zero) that C_{60} transfers to this gas molecule during their interaction.

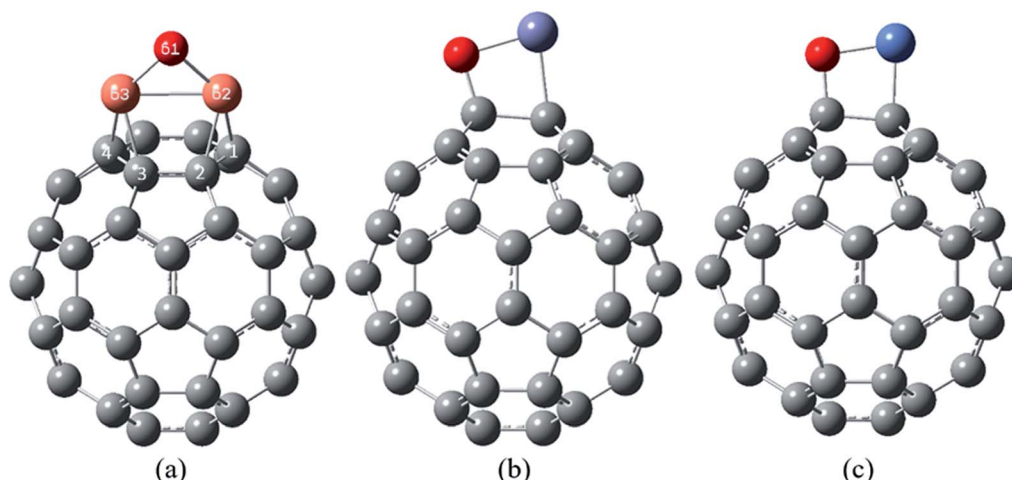


Fig. 5 The most stable complexes of (a) $\text{Cu}_2\text{O}/\text{C}_{60}$, (b) ZnO/C_{60} and (c) NiO/C_{60} , at B97D/6-311G(d,p).

Table 5 Involved bond lengths (in Å), Wiberg bond orders, in the C₆₀ and the most stable complexes of MOx/C₆₀, calculated at B97D/6-311G(d,p) level

Structure	Bond	Bond length	Bond order
Cu ₂ O/C ₆₀	Cu–O	1.817	0.493
	Cu–Cu	2.443	0.037
	Cu–C	1.970	0.295
	C–C	1.489	1.082
	C=C	1.456	1.194
ZnO/C ₆₀	Zn–O	1.944	0.282
	Zn–C	2.122	0.424
	O–C	1.408	0.994
	C–C	1.612	0.947
NiO/C ₆₀	Ni–O	1.762	0.664
	Ni–C	1.847	0.621
	O–C	1.435	0.925
	C–C	1.563	0.939
C ₆₀	C–C	1.454	1.162
	C=C	1.401	1.368

As the NBO calculations show the most significant donor–acceptor interactions in the CO/Cu₂O complex is from LP of O3 to σ^* of C1–Cu4 (78.98 kcal mol⁻¹). The strongest donor–acceptor interactions in the most stable complex of CO/ZnO are from LP of O2 to π^* of C1–O4 (102.87 kcal mol⁻¹) and to σ^* of C1–O4 (103.27 kcal mol⁻¹). In the case of CO/NiO complex, the strongest donor–acceptor interactions are from LP of O2 to σ^* of C–Ni (49.77 kcal mol⁻¹) and to σ^* of C–O3 (12.81 kcal mol⁻¹), and from LP of O3 to σ^* of C–O2 (62.68 kcal mol⁻¹).

The changes in the HOMO–LUMO levels energies of metal oxides before and after adsorption of gas molecules, along with the high values of E_{ads} , notable charge transfers during interactions, and significant changes in the enthalpy values indicate the strong interactions of the NO₂ and CO molecules with the studied MOxs. All calculations have shown that both studied gas molecules have stronger adsorption on NiO, compared to the other two MOxs.

3.3 Gases adsorption on MOx/C₆₀

3.3.1 MOx/C₆₀ complexes

Structural study. The target Cu₂O, ZnO and NiO metal oxides have been placed in different sites of the fullerene C₆₀ (on

pentagonal and hexagonal rings, on single bonds (between pentagonal and hexagonal rings) or double bonds (between two hexagonal rings)). The most stable structure for each complex of the MOx/C₆₀ (shown in Fig. 5) have been identified by calculating the E_{ads} . Harmonic vibrational frequency calculations following all the optimization calculations show that all frequencies have positive values. The calculated values of the bond lengths and Wiberg bond orders for the new formed bonds of the most stable MOx/C₆₀ complexes, along with those values for the initial C₆₀ have been listed in Table 5. The obtained E_{abs} values for these complexes have been also given in Table S1.†

The most stable structure of the Cu₂O/C₆₀ complex has been shown in Fig. 5(a). In this complex the Cu₂O molecule has located on a hexagonal ring of the C₆₀, and each of the Cu atoms has formed a quasi-trigonal ring with the atoms of the double bonds of the hexagonal ring (the bonds between hexagonal rings). This is consistent with the reports on exohedral cuprofullerenes.^{53–55} The adsorption of Cu₃ units on the C₆₀ fullerene demonstrates that each of the Cu atoms bridges on a double bond of the C₆₀ and forms a trigonal. This trend continues until the increase of eight Cu₃ units and synthesis of C₆₀@Cu₂₄.^{53,54} Also, according to the calculations, in the complex of Cu₂O/C₆₀, the Cu–O bond length is 1.817 Å, which is higher than that in a Cu₂O free molecule (1.766 Å).

In the most stable complex of ZnO/C₆₀, Fig. 5(b), the ZnO molecule has been placed exactly parallel to a bond between two hexagonal rings of the fullerene C₆₀, and has formed a quasi-tetragonal ring with the atoms of this C=C bond. According to the data in Table 5, the Zn–O bond in this complex has a calculated length of 1.944 Å, which is much longer than that in the ZnO free molecule (1.776 Å). The calculated length of new formed bonds of Zn–C and O–C in this complex are 2.122 and 1.408 Å, respectively.

Fig. 5(c) shows the most stable structure of NiO/C₆₀ complex, in which NiO (like ZnO) has posited in parallel with a C=C bond between two hexagonal rings of the C₆₀. According to the data in Tables 3 and 5, the Ni–O bond length in this complex is longer than this corresponding value in the NiO molecule. The bond lengths of Ni–C and O–C in this complex are respectively 1.847 and 1.435 Å.

AIM study. The values of ρ and $\nabla^2\rho$ at all bond critical points between the atoms involved in the interactions of the MOxs and

Table 6 Binding energies and their values with the BSSE corrections, enthalpy changes of complexation, changes of NBO charges (Δq) in MOx after complexation, ionization potential, energies of HOMO and LUMO levels and their gaps for the MOxs, and the most stable complexes of MOx/C₆₀, calculated at B97D/6-311G(d,p) level

Structure	E_{b} , (kcal mol ⁻¹)	E_{b} , + BSSE (kcal mol ⁻¹)	ΔH (kcal mol ⁻¹)	Δq (a.u.)	IP (eV)	E_{HOMO} (eV)	E_{LUMO} (eV)	Gap (eV)
Cu ₂ O/C ₆₀	-89.26	-56.07	-89.02	0.903	6.50	-4.84	-4.14	0.70
ZnO/C ₆₀	-66.93	-45.31	-66.44	0.191	6.72	-5.27	-4.18	1.09
NiO/C ₆₀	-129.42	-65.75	-128.61	0.129	6.36	-4.68	-3.99	0.69
Cu ₂ O	—	—	—	—	6.25	-3.23	-2.28	0.95
ZnO	—	—	—	—	7.84	-3.69	-3.60	0.09
NiO	—	—	—	—	5.43	-1.25	-0.59	0.66

the C_{60} have been obtained and analysed. In the most stable structure of Cu_2O/C_{60} complex, the values of $\nabla^2\rho$ and ρ at the bond critical points between the Cu atoms and the carbon atoms involved in the interaction (Fig. 5(a)) are 0.2313 and 0.0974 a.u., respectively. In the ZnO/C_{60} complex structure, the values of $\nabla^2\rho$ and ρ at the bond critical point between the oxygen and the nearest carbon atom of the C_{60} are respectively -0.6537 and 0.2748 a.u. The values of $\nabla^2\rho$ at the bond critical points between Ni and oxygen of the MOx and the nearest carbon atoms in the NiO/C_{60} complex are 0.1764 (ρ is 0.1378 a.u.) and -0.5692 (ρ is 0.2568 a.u.), respectively.

Accordingly, it can be said that the positive values of $\nabla^2\rho$ at the bond critical points between the metal-carbon show van der Waals type interactions; and relatively large and negative values of $\nabla^2\rho$ (with larger values of ρ) at the critical points between oxygen-carbon bonds display significant covalent type interactions in the studied complexes.

Energy study. The binding energies (E_b) and their corrected values for the BSSE, interaction enthalpy changes (ΔH), ionization potential (IP), energies of HOMO-LUMO and their gaps for the MOxs and the most stable MOx/ C_{60} complexes have been given in Table 6.

Comparison of the ionization potential values of the MOxs before adsorption on the C_{60} in Table 6 shows that the first ionization energy for the NiO is less than that for the other studied MOxs, therefore the NiO more easily donates electron to the C_{60} and makes stronger interaction with it.

As data in the tables show, energy of the HOMO-LUMO levels in the complexes of MOx/ C_{60} are more similar to those in the C_{60} (Table 2) in comparison with those in the MOxs. Since the fullerene C_{60} receives the electrons from the MOxs surfaces during interaction with them, its LUMO orbital surface is

expected to be involved in the interaction with the MOxs. However, since the C_{60} molecule is several times larger than the studied MOxs, its LUMO surface have not been significantly changed in the interaction with the HOMO surface of the MOxs.

Comparison between the energies of the HOMO surfaces in the MOx/ C_{60} complexes shows that the HOMO surface energy in the NiO/C_{60} complex (as the most stable complex of the studied MOx/ C_{60} complexes) relative to the HOMO in NiO has more changed in comparison with the other two cases. On the other hand, according to the data in Table 6, comparison of the calculated values of the HOMO-LUMO gaps in the fullerene C_{60} (1.66 eV) and those in the MOx/ C_{60} complexes displays that the ZnO/C_{60} complex (which is the most unstable MOx/ C_{60} complex) has less difference than the other two cases.

NBO study. Analysis of the NBO charges shows that the MOxs of the Cu_2O , ZnO and NiO have transferred a little charge to the fullerene C_{60} during interaction with it, and their total charges have become positive compared to the neutral forms before the interactions. Because NiO has a stronger interaction with the C_{60} than the other MOxs, more charge transfer during this interaction is expected. However, according to the data of Table 6, the charge transfer from the NiO to the C_{60} surface is less than that from the other two MOxs. Electron transfer process in an interaction depends extensively on the electronegativity, charge and valence electrons of the involved atoms in the interaction. The NiO and ZnO have interacted with the C_{60} by a metal atom and a non-metal electronegative oxygen atom, whereas Cu_2O has participated in the interaction through two metal atoms.

The most significant donor-acceptor interactions in the Cu_2O/C_{60} complex, are from LP of O61 to LP* of Cu62 and Cu63 atoms (that energies of both interactions are 132.51 kcal mol $^{-1}$),

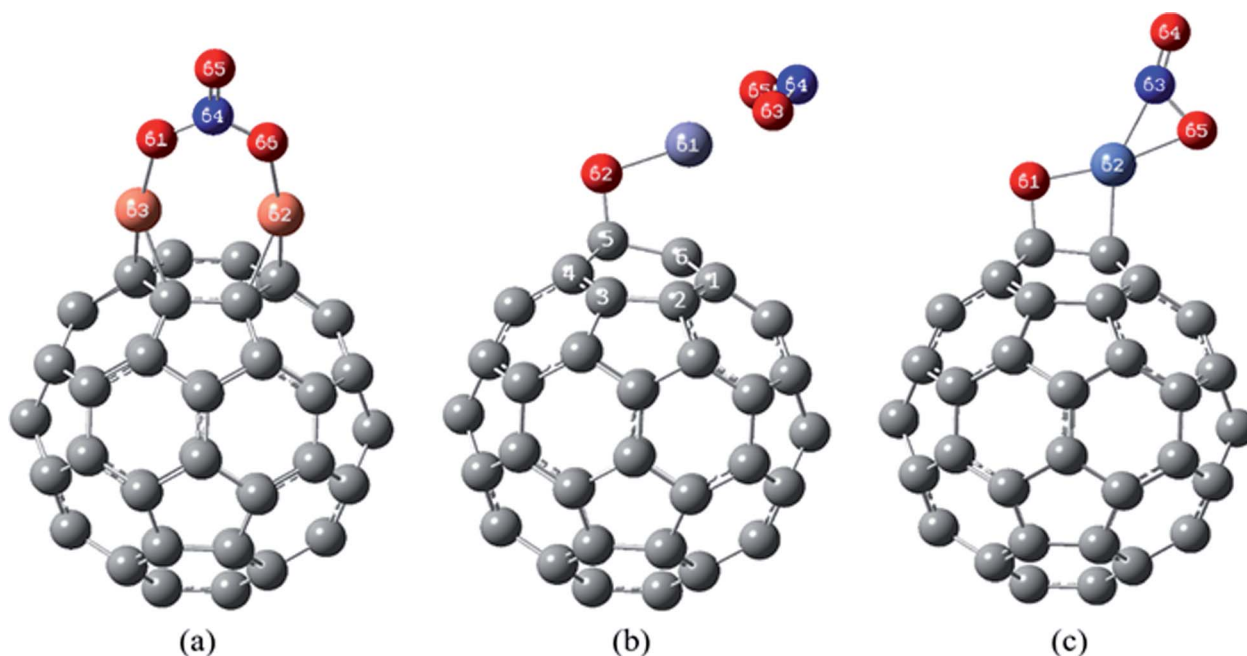


Fig. 6 The most stable complexes of (a) $NO_2/Cu_2O/C_{60}$, (b) $NO_2/ZnO/C_{60}$ and (c) $NO_2/NiO/C_{60}$, at B97D/6-311G(d,p).

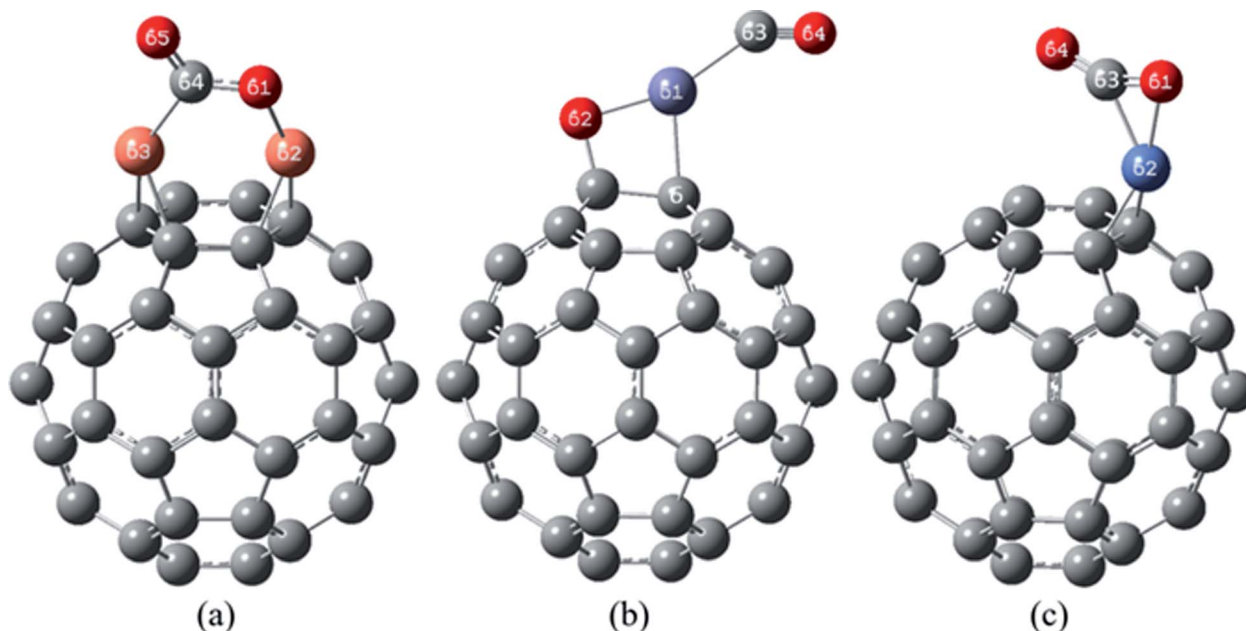


Fig. 7 The most stable complexes of (a) CO/Cu₂O/C₆₀, (b) CO/ZnO/C₆₀ and (c) CO/NiO/C₆₀, at B97D/6-311G(d,p).

also from LP of Cu62 and Cu63 atoms to π^* of C1–C2 and C3–C4 bonds, respectively (both 20.12 kcal mol⁻¹). The strongest donor–acceptor interactions in the most stable complex of ZnO/C₆₀ are from LP of O to σ^* of Zn–C and to σ^* of C–C bonds, also from σ^* of Zn–C bond to π^* of C–C bonds (27.37, 30.93 and 16.24 kcal mol⁻¹, respectively). In the case of NiO/C₆₀ complex, the strongest donor–acceptor interactions are from σ^* and σ of Ni–O bond to σ^* of Ni–C bond, from σ of Ni–C bond to π^* of C–C bonds, and from LP of O to σ^* of C–C bonds (20.66, 12.36, 19.98 and 13.16 kcal mol⁻¹, respectively).

Consequently, the high E_b s, notable charge transfers, and significant changes in the enthalpy, and the HOMO–LUMO values of the fullerene C₆₀ after adsorbing the studied MOx confirm their strong interactions. According to the mentioned calculations, the NiO/C₆₀ complex is more stable than the Cu₂O/C₆₀ and ZnO/C₆₀ complexes.

3.3.2 Gases adsorption on the MOx/C₆₀

Structural study. In order to obtain the most stable structures of NO₂/MOx/C₆₀ and CO/MOx/C₆₀ complexes, all possible structures for placing the NO₂ and CO molecules relative to the MOx/C₆₀ complexes have been considered. After optimization calculations and analysing the calculated adsorption energies for all possible structures, the given structures in Fig. 6 and 7 have been obtained as the most stable complexes.

The selected bond lengths values and their Wiberg bond orders have been given in Table 7 (and the calculated E_{abs} values have been summarized in Table S1†).

In the most stable structure of NO₂/Cu₂O/C₆₀ complex, Fig. 6(a), adsorption of the NO₂ molecule causes a significant change in the initial structure of Cu₂O/C₆₀. The two Cu atoms have formed quasi-trigonal rings with the atoms of the bonds between hexagonal rings, and oxygen atom of the Cu₂O (O61 atom) has interacted with the nitrogen atom of the NO₂ in a way

that the NO₂ molecule is oxidized to NO₃. This process can significantly reduce the volume of the NO₂ toxic gas, which is not observed in the interaction of the NO₂ on the Cu₂O.

Structure (b) in Fig. 6 shows the most stable complex of NO₂/ZnO/C₆₀, in which (similar to the most stable complex of NO₂/ZnO) NO₂ has been approached to the Zn atom from the oxygen atoms side. The distance between the Zn atom and the nearest carbon atom of the C₆₀ is 2.370 Å, which has become higher than the length of Zn–C bond in the most stable complex of ZnO/C₆₀ (2.122 Å).

The most stable structure of NO₂/NiO/C₆₀ complex has been shown in Fig. 6(c). Based on data comparison in Tables 5 and 7, in this complex, NO₂ adsorption has not significantly changed the initial structure of NiO/C₆₀ and only the length of C–Ni bond has been slightly increased. In this complex NO₂ interacts with the Ni atom through the nitrogen and one of the oxygen atoms. The values of the bond lengths and bond orders for the new formed bonds have been given in Table 7.

In the most stable structure of CO/Cu₂O/C₆₀ complex (Fig. 7(a)), adsorption of a CO molecule, like NO₂, has significantly changed the initial structure of Cu₂O/C₆₀. In the mentioned structure, the CO molecule has approached the Cu₂O from the carbon side. The two Cu atoms have formed quasi-trigonal rings with the atoms of C=C bonds between hexagonal rings. One of Cu–O bond of Cu₂O/C₆₀ has been broken, and the carbon atom of the CO has placed between these Cu and O atoms, making new bonds with both of them (the characteristics of these bonds have been given in Table 7). During this desirable process, the CO gas has relatively changed into the oxidized form of CO₂.

The most stable complex of CO/ZnO/C₆₀ has been shown in Fig. 7(b). The figure, along with the data from Tables 5 and 7 demonstrate that the initial structure of the ZnO/C₆₀ has been

Table 7 Bond lengths (in Å), Wiberg bond orders, in the most stable complexes of NO₂/MOx/C₆₀ and CO/MOx/C₆₀, calculated at B97D/6-311G(d,p) level

Structure	Bond	Bond length	Bond order
NO ₂ /Cu ₂ O/C ₆₀	Cu63–O61	1.888	0.225
	N64–O61, N64–O66	1.302	1.194
	N64–O65	1.205	1.586
	Cu62–C, Cu63–C	2.036	0.215
	Cu62–C, Cu63–C	1.973	0.253
NO ₂ /ZnO/C ₆₀	Zn61–O62	1.856	0.278
	Zn61–O63, Zn61–O65	2.096	0.205
	N64–O63, N64–O65	1.264	1.507
	O62–C	1.421	0.943
NO ₂ /NiO/C ₆₀	Zn61–C	2.370	0.080
	Ni62–O61	1.769	0.537
	Ni62–N63	1.930	0.262
	Ni62–O65	1.890	0.315
	N63–O65	1.324	1.278
	N63–O64	1.193	1.741
	Ni62–C	1.948	0.411
CO/Cu ₂ O/C ₆₀	O61–C	1.437	0.915
	Cu62–O61	1.864	0.278
	Cu63–C64	1.994	0.554
	C64–O61	1.321	1.224
	C6–O65	1.217	1.712
	Cu62–C, Cu63–C	1.976	0.342
CO/ZnO/C ₆₀	Cu62–C, Cu63–C	2.200	0.140
	Zn61–O62	1.860	0.290
	Zn61–C63	2.009	0.347
	C63–O64	1.146	2.246
CO/NiO/C ₆₀	Zn61–C	2.087	0.238
	O62–C	1.430	0.948
	Ni62–O61	1.898	0.304
	Ni62–C63	1.891	0.521
	O61–C63	1.253	1.496
	C63–O64	1.187	1.846
	Ni62–C	1.929	0.393

maintained after CO adsorption. The distances of Zn and O atoms to carbon atoms of the C₆₀ in CO/ZnO/C₆₀ are greatly comparable to those in the most stable complex of the ZnO/C₆₀. In this structure, the CO molecule has interacted with the Zn atom from the carbon atom side, and the distance between Zn and carbon of the CO is 2.009 Å (with a bond order of 0.347).

Fig. 7(c) shows the most stable structure of CO/NiO/C₆₀ complex. According to the data of Tables 5 and 7, in this

structure, adsorption of the CO causes significant changes in the initial structure of NiO/C₆₀ (Fig. 5(c)). In the mentioned structure, the NiO has interacted with the C₆₀ only by its Ni atom in such way that has formed a quasi-trigonal ring with the carbon atoms of a C=C bond between two hexagonal rings of the C₆₀. The CO molecule has approached the NiO molecule from its carbon side and has interacted extensively with the both O and Ni atoms. In this complex, the distance between the carbon atom of CO to the oxygen atom of the NiO/C₆₀ unit is 1.253 Å (with bond order of 1.496), which indicates the strong interaction of the CO molecule with the complex of NiO/C₆₀ and the relatively oxidation of the CO to the CO₂.

AIM study. The values of ρ and $\nabla^2\rho$ at all bond critical points between the atoms involved in the interactions of the target gas molecules and the MOx/C₆₀ have been analysed. In the NO₂/Cu₂O/C₆₀ complex, according to the obtained data from the AIM calculations, the $\nabla^2\rho$ value at the critical point of the bond between the N and the O61 (of the metal oxide) is exactly equal to that between the N and the O66 (of the initial NO₂). The magnitude and sign of the mentioned Laplacian (−0.5760, with $\rho = 0.4093$ a.u.) confirm two strong covalent interactions.

In the most stable complex of NO₂/ZnO/C₆₀, the $\nabla^2\rho$ value for the bond between the Zn and the oxygen of NO₂, which is 0.2529 (with $\rho = 0.0637$ a.u.), shows a van der Waals type interaction between the NO₂ and ZnO/C₆₀ in this complex.

In the case of NO₂/NiO/C₆₀ complex, the $\nabla^2\rho$ value at the bond critical point between the Ni and the N atoms is 0.4779 ($\rho = 0.0966$ a.u.).

In the most stable structure of CO/Cu₂O/C₆₀ complex, the value of $\nabla^2\rho$ at the critical point of C64–O61 bond is −0.4466 ($\rho = 0.3139$ a.u.). These magnitude and sign indicate a strong covalent interaction in this gas adsorption.

In the CO/ZnO/C₆₀ complex, the $\nabla^2\rho$ and ρ values (0.2175 and 0.0884 a.u., respectively) at the bond critical point between carbon atom of the gas molecule and the Zn of the metal oxide show a van der Waals type interaction between CO and ZnO/C₆₀.

For the CO/NiO/C₆₀ complex, the calculated values of $\nabla^2\rho$ at the critical points of Ni–C63 and O61–C63 bonds (in Fig. 7(c)) are respectively 0.2429 ($\rho = 0.1189$ a.u.) and −0.3324 ($\rho = 0.3701$ a.u.), that the negative value of $\nabla^2\rho$ (with relatively large value of ρ) also confirms the strong covalent interaction between the carbon of the CO gas and the oxygen of the NiO metal oxide.

Energy study. The values of E_{ads} , with the BSSE corrections, the enthalpy changes, energies of the HOMO–LUMO levels and

Table 8 Adsorption energies and their values with the BSSE corrections, enthalpy changes of complexation, changes of NBO charges (Δq) in NO₂ and CO after complexation, energies of HOMO and LUMO levels and their gaps for the most stable complexes of NO₂/MOx/C₆₀ and CO/MOx/C₆₀, calculated at B97D/6-311G(d,p) level

Structure	E_{ads} , (kcal mol ^{−1})	$E_{\text{ads.}} + \text{BSSE}$ (kcal mol ^{−1})	ΔH (kcal mol ^{−1})	Δq (a.u.)	E_{HOMO} (eV)	E_{LUMO} (eV)	Gap (eV)
NO ₂ /Cu ₂ O/C ₆₀	−32.98	−19.36	−30.70	−0.553	−5.28	−4.31	0.97
NO ₂ /ZnO/C ₆₀	−53.36	−45.99	−52.08	−0.651	−5.34	−4.18	1.16
NO ₂ /NiO/C ₆₀	−53.68	−62.30	−52.58	−0.492	−5.59	−4.34	1.25
CO/Cu ₂ O/C ₆₀	−36.32	−28.17	−33.83	−0.206	−4.81	−4.00	0.80
CO/ZnO/C ₆₀	−18.42	−10.07	−17.08	−0.170	−5.17	−4.20	0.97
CO/NiO/C ₆₀	−82.27	−71.12	−80.01	0.234	−5.57	−4.12	1.45

their related gaps for the most stable complexes of NO₂/MOx/C₆₀ and CO/MOx/C₆₀ have been calculated and the results have been summarized in Table 8.

The calculated energies for adsorption of the NO₂ and CO gases on the studied complexes of MOx/C₆₀ show the much bigger values, compared to the values of the adsorption energies of these gas molecules on the C₆₀ (Table 2). The high values of enthalpy changes in these interactions are also another confirmation of the strength of these adsorption processes compared to those that occur on the C₆₀. Moreover, these enthalpy changes with negative sign indicate that these adsorption processes are exothermic.

According to the calculated Δq in Table 8, during gas adsorptions on the MOx/C₆₀, some charge transfer is occurred from the MOx/C₆₀ to the gases. For this, the LUMO of the NO₂ is involved in the interaction with the HOMOs of the MOx/C₆₀ complexes. According to the data in Tables 6 and 8, after NO₂ adsorption, the energy changes in the HOMO levels of the MOx/C₆₀ complexes are more than that in their LUMO levels, which is in agreement with the charge transfer from the HOMO of the MOx/C₆₀ complexes. According to the calculated data, in comparison to the other two MOx/C₆₀ complexes, the HOMO level in the NiO/C₆₀ complex is closer to the LUMO level of the NO₂ molecule, which results in a stronger interaction between them. The changes in energy of the HOMO surfaces and the HOMO–LUMO gaps in MOx/C₆₀ complexes, after NO₂ adsorption, are much more significant in comparison with the corresponding changes in the C₆₀ (Table 2).

According to data in Tables 6 and 8, in comparison to the other CO/MOx/C₆₀ complexes, both HOMO and LUMO levels in the CO/NiO/C₆₀ complex have become more stable during gas adsorption. The change in the HOMO–LUMO gap value before and after CO adsorption on the NiO/C₆₀ complex is also greater than those on the other MOx/C₆₀ complexes, which confirm the stronger adsorption of this gas molecule on the NiO/C₆₀ complex.

NBO study. According to the NBO charge changes, given in Table 8, the total charge of the NO₂ molecule has become negative after adsorption on the MOx/C₆₀ complexes, which indicates the electron transfer from these complexes to the NO₂. Because the NiO/C₆₀ has a stronger interaction with the NO₂ than the other MOx/C₆₀ complexes, more charge transfer is expected during this adsorption process. However, according to

the Table 8, the charge transfer for the interaction of NO₂ with ZnO/C₆₀ is higher than the other two cases. As mentioned, NO₂ has interacted with the ZnO/C₆₀ from the oxygen atoms side. Since oxygen has a high electronegativity, NO₂ receives more electrons from the ZnO/C₆₀ surface during adsorption on it. Comparison between the ionization potential of MOx/C₆₀ complexes before NO₂ adsorption in Table 6 shows that the IP for NiO/C₆₀ is lower than those for the other MOx/C₆₀ complexes, and therefore NiO/C₆₀ more easily donates its first electron to the NO₂ and interacts more strongly with it.

Based on the NBO results, donor–acceptor interactions are in agreement to the charge transfers during these processes, and confirm the changes of atomic charges. The most notable donor–acceptor interactions in the complex of NO₂/Cu₂O/C₆₀ are from LP of O61 and O66 atoms to σ^* of N64–O65 bond (both 28.76 kcal mol⁻¹). In the case of NO₂/ZnO/C₆₀ complex the most significant interactions is from LP of O62 atom to LP* of Zn61 atom (34.00 kcal mol⁻¹). These interactions in the NO₂/NiO/C₆₀ are from LP of O61 atom to LP* of Ni62, from σ^* of C–Ni62 to LP* of Ni62 atom, and from LP of O65 to σ^* of N63–O64 (36.66, 22.03 and 26.27 kcal mol⁻¹, respectively).

In the complexes of CO/Cu₂O/C₆₀ and CO/ZnO/C₆₀, the electrons has been transferred to the CO gas throughout the bond formed between its C atom and the metal atom of the MOx, and (according to the NBO charge calculations) the total charge of the CO molecule has become negative after adsorption on the Cu₂O/C₆₀ and ZnO/C₆₀ complexes. In the complex of CO/NiO/C₆₀, the CO molecule has reasonably changed into a CO₂ molecule by creating a strong covalent bond with the oxygen (non-metal) atom of the NiO, but tendency of the mentioned oxygen to keep a bond with the Ni prevents releasing of that as the free CO₂.

According to the NBO calculations, donor–acceptor interactions also confirm the charge transfer processes. Interactions from LP of O61 atom to π^* and to σ^* of C64–O65 bond (14.11 and 26.01 kcal mol⁻¹, respectively) in the CO/Cu₂O/C₆₀, and from σ^* of C6–Zn61 to LP* of C63 atom (47.64 kcal mol⁻¹) in the CO/ZnO/C₆₀ are some examples. In the complex of CO/NiO/C₆₀, the most notable interactions are from LP of O64 atom to σ^* of Ni62–C63 bond, from σ^* of Ni62–C63 to LP* of Ni62 atom (97.71 and 60.38 kcal mol⁻¹, respectively), and from LP of O61 atom to σ^* of C63–O64 and Ni62–C63 bonds (71.57 and 67.52 kcal mol⁻¹, respectively).

Table 9 Calculated values of polarizability (α) and HOMO–LUMO gap for C₆₀, MOxs and the most stable complexes of MOx/C₆₀ adsorbents, at B97D/6-311G(d,p) level, along with their experimental values

Structure	$\alpha_{\text{calc.}}$ ($^3\text{\AA}$)	$\alpha_{\text{exp.}}$ ($^3\text{\AA}$) ^a	Gap _{calc.} (eV)	Gap _{exp.} (eV)
C ₆₀	75.79	76.50 ± 0.80 (ref. 63)	1.66	1.80–1.60 (ref. 56)
Cu ₂ O	6.68	6.54 (ref. 65)	0.95	2.28 (ref. 57)
ZnO	2.31	2.61 (ref. 64)	0.09	3.37 (ref. 58)
NiO	1.35	2.20 (ref. 64)	0.66	4.00 (ref. 60)
Cu ₂ O/C ₆₀	87.92	—	0.70	—
ZnO/C ₆₀	87.35	—	1.09	—
NiO/C ₆₀	83.59	—	0.69	—

^a By empirical findings and Lorentz–Lorenz relation.

Comparing the data in Tables 2 and 8 clearly demonstrate that amount of charge transfer during gas adsorption for the MOx/C₆₀ complexes is higher than that for the C₆₀.

Consequently, the high E_{ads} , significant charge transfers during interactions, and notable changes in the enthalpy values, energies of HOMO–LUMO levels and their gaps for the MOx/C₆₀ complexes after adsorption of the NO₂ and CO gases indicate strong interactions between these gas molecules and the MOx/C₆₀ complexes compared to the weak interactions between them and the fullerene C₆₀.

3.4 Investigation of some reactivity indices in the studied adsorbents

The values of the HOMO–LUMO gap for the fullerene C₆₀ (ref. 56) and the Cu₂O,⁵⁷ ZnO⁵⁸ and NiO^{59,60} have been measured during various experiments. These experimental values along with their calculated values in the present study have been given in Table 9.

According to the data in this table, the calculated value of HOMO–LUMO gap for the C₆₀ at the theoretical level of B97D/6-311G (d,p) is in good agreement with the experimental value.⁵⁶ On the other hand, in the case of the studied MOx, their calculated gap values are much lower than their experimental values. Despite the remarkable successes of DFT theory in the framework of LDA and GGA approximations, these methods are incapable for prediction some parameters related to the strongly correlated systems.^{61,62} The reason is misbehavior of the exchange interactions in these approximations, which do not sufficiently eliminate the electron self-interaction errors, and therefore estimate the energy values of the unoccupied surfaces (LUMO) less than the actual values.⁶¹ Because the intermediate MOx are the most prominent examples for the strongly correlated systems, the calculated values of their HOMO–LUMO gap using DFT methods are much smaller than the actual values and are not reliable.^{61,62}

Since the calculated values of the HOMO–LUMO gap for the MOx molecules are not enough accurate, the study of parameters such as chemical hardness or chemical potential, that are directly related to the HOMO–LUMO gap, are not suitable for checking the stability or reactivity of the studied adsorbent species. The polarizability parameter is one of the reliable indices in computational methods and also determines the chemical hardness of considered systems. The more realistic values of polarizability using empirical findings and Lorentz–Lorenz equation for the C₆₀ (ref. 63) and all three MOx molecules (NiO,⁶⁴ ZnO⁶⁴ and Cu₂O⁶⁵) have been given in Table 9. These values are reasonably consistent with the calculated values here at the studied theoretical level.

According to the obtained data for the polarizability, it can be clearly seen that the adsorbents containing the C₆₀ are much softer than the MOx adsorbents, and it is predicted that they exhibit higher conductivity and reactivity. In addition, organic compounds (such as fullerenes) are more readily modified than inorganic materials (including MOx) and it is expected the MOx/C₆₀ complexes would be better detectors or

filters for the gas species including CO and NO₂ in comparison with the MOx nanoparticles which have very low selectivity.^{66,67}

Interaction between organic–inorganic interfaces alternates electronic states, bond gap and magnetic moment of the substrates. For example, the presence of fullerene in CdSe–C₆₀ nanocomposites allows energy levels and band gap of the system to be adjusted by resizing CdSe substrate.⁶⁸ In the reaction between the surfaces of C₆₀ and tungsten (W), the bond gap can be controlled by selecting the annealing temperature.⁶⁹ These are just some example of the bond gap engineering. A selective substrate for adsorption of gases or vapors can be achieved by bond gap engineering in gas adsorbents combined with modified fullerene.^{70–74} Other example is modifying polyphenylene oxide membranes (PPO) with fullerene that exhibits a lower gas permeability and enhanced selectivity for gas separation in comparison with the PPO.⁷⁰ Combining polystyrene with the fullerene C₆₀, as a hybrid gas separation membrane, leads to a change in the crystallinity, density, and free volume in this membrane. This improve some transport properties which in turn leads to an improvement of the selectivity in the gas separation.⁷¹ Therefore, the modified MOx/C₆₀ complexes are expected to show more potent in selectivity of gas adsorptions.

4 Conclusions

Combination of fullerene and MOx, to make composite nanostructures, are interesting not only because they display the individual properties of fullerene and MOx nanoparticles but they may also exhibit synergetic properties that are advantageous for gas sensing applications. The studied MOx molecules, during adsorption on the fullerene C₆₀ surface, transfer some electrons to the C₆₀. High adsorption energies, significant changes in the both enthalpy and the HOMO–LUMO values of the fullerene C₆₀, after adsorption of the MOx, indicate strong interactions in the resulting MOx/C₆₀ complexes. According to calculations, the NiO is more stably absorbed on the surface of the C₆₀ than the Cu₂O and ZnO.

According to the results, the MOx/C₆₀ complexes are much stronger adsorbents than the C₆₀ in the gas adsorption. The charge transfers to the NO₂ and CO gas molecules from the MOx/C₆₀ complexes are much more significant compared to those from C₆₀. The calculated adsorption energies and the enthalpy changes for adsorption of the studied gas molecules on the MOx/C₆₀ complexes are several times larger than those on the C₆₀. These adsorptions on the NiO/C₆₀ are stronger than on the other MOx/C₆₀ complexes.

According to the obtained data for the polarizability, it can be clearly seen that the adsorbents containing the C₆₀ are much softer than the MOx adsorbents, and it is predicted that they exhibit higher conductivity and reactivity. Although the MOx/C₆₀ complexes are weaker adsorbents for the NO₂ and CO gases in comparison with the MOx, but because the organic compounds (such as fullerenes) are more readily modified than inorganic materials (including MOx), the MOx/C₆₀ complexes are more potent in selectivity of adsorption of different gases,

such as CO and NO₂, and they may require lower operating temperatures than the MOx.

It is expected that combination of the MOx and the C₆₀ three-dimensional system, with the rapid recombination of electron-hole pairs, reduction photo-corrosion processes, also with increase the interaction area surface, would provide ideal gaseous adsorbents with more stability than the MOx adsorbents.

Author contributions

A-Reza Nekoei: supervision, conceptualization, methodology, resources, writing-review & editing. Sanaz Haghgoo: conceptualization, formal analysis, investigation, writing-original draft.

Conflicts of interest

There are no conflicts to declare.

References

- 1 R. Aitken, M. Q. Chaudhry, A. B. A. Boxall and M. Hull, *Occup. Med.*, 2006, **56**, 300–306.
- 2 K. I. Hadjiivanov and D. K. Klissurski, *Chem. Soc. Rev.*, 1996, **25**, 61–69.
- 3 W. T. Qiao, G. W. Zhou, X. T. Zhang and T. D. Li, *Mater. Sci. Eng. Carbon*, 2009, **29**, 1498–1502.
- 4 D. L. Jiang, S. Q. Zhang and H. J. Zhao, *Environ. Sci. Technol.*, 2007, **41**, 303–308.
- 5 H. S. Yun, K. Miyazawa, I. Honma, H. S. Zhou and M. Kuwabara, *Mater. Sci. Eng. Carbon*, 2003, **23**, 487–494.
- 6 N. Todorova, T. Giannakopoulou and T. Vaimakis, *Mater. Sci. Eng., B*, 2008, **152**, 50–54.
- 7 G. P. Lepore, C. H. Langford, J. Vichova and A. Vlcek, *J. Photochem. Photobiol., A*, 1993, **75**, 67–75.
- 8 S. Fukuzumi, K. M. Kadish, K. Smith and R. Guilard, in *The Porphyrin Handbook: Inorganic, Organometallic and Coordination Chemistry*, Academic Press, San Diego, 2000.
- 9 L. Echegoyen and L. E. Echegoyen, *Acc. Chem. Res.*, 1998, **31**, 593–601.
- 10 S. Fukuzumi and D. M. Guldi, in *Electron Transfer in Chemistry: Electron-Transfer Chemistry of Fullerenes*, ed. V. Balzani, Wiley-VCH, Weinheim, 2001, p. 270.
- 11 S. Fukuzumi and H. Imahori, in *Electron Transfer in Chemistry: Electron-Transfer Chemistry of Fullerenes*, ed. V. Balzani, Wiley-VCH, Weinheim, 2001, p. 927.
- 12 M. Melle-Franco, M. Marceccio, D. Paolucci, F. Paolucci, V. Georgakilas and D. Guldi, *J. Am. Chem. Soc.*, 2004, **126**, 1646–1647.
- 13 T. G. Nenov and S. P. Yordanov, *Ceramic Sensors-Technology and Applications*, Technomic Publishing, Lancaster, PA, 1996.
- 14 H. Meixner and U. Lampe, *Sens. Actuators, B*, 1996, **33**, 198–202.
- 15 P. T. Moseley, *Meas. Sci. Technol.*, 1997, **8**, 223–237.
- 16 B. Cao and W. J. Cai, *J. Phys. Chem. C*, 2008, **112**, 680–685.
- 17 Q. Li, V. Kumar, Y. Li, H. Zhang, T. J. Marks and R. P. H. Chang, *Chem. Mater.*, 2005, **17**, 1001–1006.
- 18 S. Zhang, H. S. Chen, K. Matras-Postolek and P. Yang, *Phys. Chem. Chem. Phys.*, 2015, **17**, 30300–30306.
- 19 M. H. Huang, S. Mao, H. Feick, H. Yan, Y. Wu, H. Kind, E. Weber, R. Russo and P. Yang, *science*, 2001, **292**, 1897–1899.
- 20 S. G. Chatterjee, S. Chatterjee, A. K. Ray and A. K. Chakraborty, *Sens. Actuators, B*, 2015, **221**, 1170–1181.
- 21 Z. D. Meng, L. Zhu, J. G. Choi, M. L. Chen and W. C. Oh, *J. Mater. Chem.*, 2011, **21**, 7596–7603.
- 22 H. Fu, T. Xu, S. Zhu and Y. Zhu, *Environ. Sci. Technol.*, 2008, **42**, 8064–8069.
- 23 S. B. Lovern and R. Klaper, *Environ. Toxicol. Chem.*, 2006, **25**, 1132–1137.
- 24 A. Martínez-Alonso, J. M. D. Tascón and E. J. Bottani, *J. Phys. Chem. B*, 2001, **105**, 135–139.
- 25 A. M. El Mahdy, *Appl. Surf. Sci.*, 2016, **383**, 353–366.
- 26 B. Gao, J. X. Zhao, Q. H. Cai, X. G. Wang and X. Z. Wang, *J. Phys. Chem. A*, 2011, **115**, 9969–9976.
- 27 M. Luo, Z. Liang, S. G. Peera, M. Chen, C. Liu, H. Yang, J. Liu, U. P. Kumar and T. Liang, *Appl. Surf. Sci.*, 2020, **525**, 146480.
- 28 M. Luo, Z. Liang, M. Chen, C. Liu, X. Qi, S. G. Peera, J. Liu and T. Liang, *New J. Chem.*, 2020, **44**, 15724–15732.
- 29 M. Luo, Z. Liang, C. Liu, X. Qi, M. Chen, H. Yang and T. Liang, *RSC Adv.*, 2020, **10**, 27856–27863.
- 30 M. Luo, Z. Liang, C. Liu, M. Liu, X. Qi, M. Chen, H. Yang and T. Liang, *ACS Omega*, 2020, **5**, 21203–21210.
- 31 M. Luo, Z. Liang, M. Chen, S. G. Peera, C. Liu, H. Yang, X. Qi, J. Liu and T. Liang, *New J. Chem.*, 2020, **44**, 9402–9410.
- 32 M. Luo, Z. Liang, C. Liu, X. Qi, M. Chen, R. U. R. Sagar, H. Yang and T. Liang, *Appl. Surf. Sci.*, 2021, **536**, 147809.
- 33 B. Son, W. Yang, P. Breysse, T. Chung and Y. Lee, *Environ. Res.*, 2004, **94**, 291–296.
- 34 Report on a WHO Working Group, *Health Aspects of Air Pollution with Particulate Matter, Ozone and Nitrogen Dioxide*, Bonn, Germany, 2003, vol. 13–15.
- 35 Y. Xie, Y. P. Huo and J. M. Zhang, *Appl. Surf. Sci.*, 2012, **258**, 6391–6397.
- 36 M. Shelef, *Chem. Rev.*, 1995, **95**, 209–225.
- 37 S. L. Schroeder and M. Gottfried, *Adv. Phys. Chem. Lab.*, 2002, 1–22.
- 38 S. Grimme, *J. Comput. Chem.*, 2006, **27**, 1787–1799.
- 39 F. B. Van Duijneveldt, J. G. van Duijneveldt-van de Rijdt and J. H. van Lenthe, *Chem. Rev.*, 1994, **94**, 1873–1885.
- 40 D. W. Schwenke and D. G. Truhlar, *J. Chem. Phys.*, 1985, **82**, 2418–2426.
- 41 M. J. Frisch, G. W. Trucks, H. B. Schlegel, G. E. Scuseria, M. A. Robb, J. R. Cheeseman, G. Scalmani, V. Barone, B. Mennucci, G. A. Petersson, H. Nakatsuji, M. Caricato, X. Li, H. P. Hratchian, A. F. Izmaylov, J. Bloino, G. Zheng, J. L. Sonnenberg, M. Hada, M. Ehara, K. Toyota, R. Fukuda, J. Hasegawa, M. Ishida, T. Nakajima, Y. Honda, O. Kitao, H. Nakai, T. Vreven, J. A. Montgomery, J. E. Peralta, F. Ogliaro, M. Bearpark, J. J. Heyd, E. Brothers, K. N. Kudin, V. N. Staroverov, R. Kobayashi, J. Normand, K. Raghavachari, A. Rendell, J. C. Burant,

- S. S. Iyengar, J. Tomasi, M. Cossi, N. Rega, J. M. Millam, M. Klene, J. E. Knox, J. B. Cross, V. Bakken, C. Adamo, J. Jaramillo, R. Gomperts, R. E. Stratmann, O. Yazyev, A. J. Austin, R. Cammi, C. Pomelli, J. W. Ochterski, R. L. Martin, K. Morokuma, V. G. Zakrzewski, G. A. Voth, P. Salvador, J. J. Dannenberg, S. Dapprich, A. D. Daniels, O. Farkas, J. B. Foresman, J. V. Ortiz, J. Cioslowski and D. J. Fox, *Gaussian 09, Revision D.01*, Wallingford CT, 2013.
- 42 E. D. Glendening, J. K. Badenhoop, A. E. Reed, J. E. Carpenter, J. A. Bohmann, C. M. Morales and F. Weinhold, *NBO 5.0, Theoretical Chemistry Institute, University of Wisconsin*, Madison WI, 2001.
- 43 R. Dennington, T. Keith and J. Millam, *GaussView Version 5*, Semichem Inc., Shawnee Mission KS, 2009.
- 44 F. W. Biegler König, J. Schonbohm and D. Bayles, *AIM2000, J. Comput. Chem.*, 2001, **22**, 545–559.
- 45 R. F. Bader and H. Essén, *J. Chem. Phys.*, 1984, **80**, 1943–1960.
- 46 L. E. Sutton, *J. Chem. Soc.*, 1965, 1956–1959.
- 47 C. B. Leffert, W. M. Jackson and E. W. Rothe, *J. Chem. Phys.*, 1973, **58**, 5801–5806.
- 48 M. Spencer, I. Yarovsky, W. Wlodarski and K. Kalantar-Zadeh, in *Solid-State Sensors, Actuators and Microsystems Conference*, 2007, pp. 987–990.
- 49 B. Wang, J. Nisar and R. Ahuja, *ACS Appl. Mater. Interfaces*, 2012, **4**, 5691–5697.
- 50 X. Zhao, X. Ren, R. Zhu, Z. Luo and B. Ren, *Aquat. Toxicol.*, 2016, **180**, 56–70.
- 51 C. T. Ng, L. Q. Yong, M. P. Hande, C. N. Ong, L. E. Yu, B. H. Bay and G. H. Baeg, *Int. J. Nanomed.*, 2017, **12**, 1621–1637.
- 52 J. C. Lavalley, J. Saussey and T. Rais, *J. Mol. Catal.*, 1982, **17**, 289–298.
- 53 S. Z. Zhan, G. H. Zhang, J. H. Li, J. L. Liu, S. H. Zhu, W. Lu, J. Zheng, S. W. Ng and D. Li, *J. Am. Chem. Soc.*, 2020, **142**, 5943–5947.
- 54 D. Chu, Y. Liu, Y. Li, Y. Liu and Y. Cui, *Inorg. Chem. Front.*, 2020, **7**, 2556–2559.
- 55 S. Z. Zhan, J. H. Li, Y. Li, G. Xu, D. F. Luo, L. Dang and D. Li, *Sci. China Mater.*, 2021, 1–7, DOI: 10.1007/s40843-020-1589-7.
- 56 C. H. Andersson, *Chemistry of Carbon Nanostructures: Functionalization of Carbon Nanotubes and Synthesis of Organometallic Fullerene Derivatives, Doctoral dissertation*, Uppsala University, 2011.
- 57 I. Grozdanov, *Mater. Lett.*, 1994, **19**, 281–285.
- 58 Z. L. Wang, *J. Phys.: Condens. Matter*, 2004, **16**, R829–R858.
- 59 S. Hüfner, J. Osterwalder, T. Riesterer and F. Hulliger, *Solid State Commun.*, 1984, **52**, 793–796.
- 60 G. A. Sawatzky and J. W. Allen, *Phys. Rev. Lett.*, 1984, **53**, 2339–2342.
- 61 R. Gillen and J. Robertson, *J. Phys.: Condens. Matter*, 2013, **25**, 165502.
- 62 J. P. Perdew and A. Zunger, *Phys. Rev. B*, 1981, **23**, 5048–5079.
- 63 R. Antoine, P. Dugourd, D. Rayane, E. Benichou, M. Broyer, F. Chandezon and C. Guet, *J. Chem. Phys.*, 1999, **110**, 9771–9772.
- 64 V. Dimitrov and S. Sakka, *J. Appl. Phys.*, 1996, **79**, 1736–1740.
- 65 A. C. Lasaga and R. T. Cygan, *Am. Mineral.*, 1982, **67**, 328–334.
- 66 S. Zampolli, I. Elmi, J. Stürmann, S. Nicoletti, L. Dori and G. C. Cardinali, *Sens. Actuators, B*, 2005, **105**, 400–406.
- 67 B. Bahrami, A. Khodadadi, M. Kazemeini and Y. Mortazavi, *Sens. Actuators, B*, 2008, **133**, 352–356.
- 68 S. Sarkar, B. Rajbanshi and P. Sarkar, *J. Appl. Phys.*, 2014, **116**, 114303.
- 69 E. Monazami, J. B. McClimon, J. Rondinelli and P. Reinke, *ACS Appl. Mater. Interfaces*, 2016, **8**, 34854–34862.
- 70 G. A. Polotskaya, D. V. Andreeva and G. K. El'yashevich, *Tech. Phys. Lett.*, 1999, **25**, 555–557.
- 71 A. Y. Pulyalina, V. A. Rostovtseva, Z. Pientka, L. V. Vinogradova and G. A. Polotskaya, *Pet. Chem.*, 2018, **58**, 296–303.
- 72 V. A. Karachevtsev, A. M. Plokhotnichenko, V. A. Pashynska, A. Y. Glamazda, O. M. Vovk and A. M. Rao, *Appl. Surf. Sci.*, 2007, **253**, 3062–3065.
- 73 H. B. Lin and J. S. Shih, *Sens. Actuators, B*, 2003, **92**, 243–254.
- 74 S. Keshtkar, A. Rashidi, M. Kooti, M. Askarieh, S. Pourhashem, E. Ghasemy and N. Izadi, *Talanta*, 2018, **188**, 531–539.